RIS LOCALIZATION AND SPATIALLY WIDEBAND FILTERING EFFECTS

Dario Tagliaferri, Marouan Mizmizi, Silvia Mura, Umberto Spagnolini

Dipartimento di Elettronica, Informazione e Bioingegneria, Politecnico di Milano, 20133 Milano, Italy

ABSTRACT

Reconfigurable intelligent surfaces (RISs) have been considered recently for target localization. While existing literature typically uses fixed RISs in the environment, mounting RISs on targets is a novel approach that can improve target visibility and positioning. This study derives the Cramér-Rao bound (CRB) for pose estimation (i.e., RIS position and orientation) under a generic wideband and near-field model. The theoretical findings show that a pose-dependent filtering phenomenon occurs, impacting the CRB, which is neglected under narrowband approximation. The extent of this effect varies based on factors such as RIS dimensions and signal bandwidth.

Index Terms— RIS, localization, Cramér-Rao bound, near-field, spatially wideband effects

1. INTRODUCTION

Reconfigurable intelligent surfaces (RISs) are discrete meta-surfaces made of passive regularly spaced, sub-wavelength-sized elements whose reflection coefficient can be dynamically tuned to manipulate the direction of reflection and refraction of an impinging wave [1]. The usage of RIS in the sensing context is relatively recent [2]. In [3], the authors proposed to use a RIS to assist radar in non-line-of-sight conditions, focusing on the probability of correct detection. The Cramér-Rao bound (CRB) on position estimation is also reported. The work [4] considers indoor localization by means of wall-placed RIS. With the advent of large RISs, research efforts focused on near-field (NF) propagation, namely considering the wavefront curvature across the RIS. NF operation opened for further research on fundamental localization bounds and practical RIS phase configuration. The work [5] derives the CRB for position and orientation estimation in some selected practical cases, assuming NF operating conditions and discussing the phase configuration. The authors of [6] propose a practical NF RIS phase configuration and analyze the CRB on position estimation. In all the aforementioned literature, RISs are fixed in the environment. In some scenarios, however, the RIS can be directly lodged on

targets, to enhance their "visibility" in the sensing data and ease their localization. This setup for RIS localization is only considered in [7] and [8]. In the former, the authors investigate the CRB on position and orientation estimation for a target-mounted RIS under far-field (FF) assumption, while the latter addresses the CRB evaluation on position estimation with a perfect RIS phase configuration and bistatic settings. Nonetheless, none of the prior studies assess the implications of *spatially wideband* phenomena, which alter the RIS response as signal frequency shifts within the utilized bandwidth, resulting in either reflection beam squinting (FF) or defocusing (NF). The only work addressing this issue is [9], albeit focusing on an RIS fixed within the environment.

This paper tackles the problem of 3D position plus 3D orientation (i.e., pose) estimation of a RIS, that can be possibly located on a desired target, in a generic bistatic, NF, and spatially wideband setting. We derive the CRB, outlining the importance of considering the wideband RIS behavior in practical cases, where the RIS acts as a *pose-dependent filter* for the impinging sensing signal. Remarkably, the latter effect allows increasing or reducing the available information w.r.t. the narrowband case (where the RIS is assumed to behave like a frequency-independent target) depending on the RIS size and the specific employed bandwidth value.

The paper is organized as follows: Sect. 2 presents the system model, in Sect. 3 we evaluate the CRB, Sect. 4 presents the numerical results while Sect. 5 concludes the paper. We adopt the following notation: bold upper- and lower-case denote matrices and column vectors. The L2-norm of a vector is denoted with $\| \cdot \|$. Matrix transposition and conjugate transposition are indicated respectively as $\mathbf{A}^T$ and $\mathbf{A}^H$. $\mathbf{I}_n$ is the identity matrix of size n. $\mathbf{a} \sim \mathcal{CN}(\boldsymbol{\mu}, \mathbf{C})$ denotes a multi-variate circularly complex Gaussian random variable with mean $\boldsymbol{\mu}$ and covariance $\mathbf{C}$. $\mathrm{trace}(\mathbf{A})$ extracts the trace of $\mathbf{A}$. $\mathbb{R}$ and $\mathbb{C}$ stand for the set of real and complex numbers, respectively. δ_n is the Kronecker delta.

2. SYSTEM MODEL

Let us consider a generic sensing terminal in a bistatic setting (e.g., a multiple-input multiple-output (MIMO) radar) that aims at estimating the position and orientation of a target equipped with a RIS (Fig. 1). In a *global* reference system, the phase centers of transmitting (Tx) and receiving (Rx)
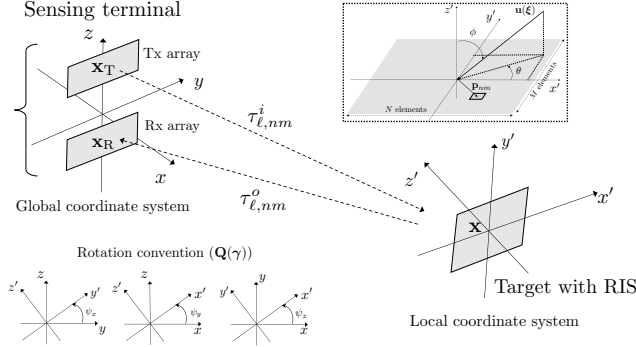
Fig. 1: System model.

antenna arrays are located in $\mathbf{x}_\mathrm{T} \in \mathbb{R}^{3\times1}$ and $\mathbf{x}_\mathrm{R} \in \mathbb{R}^{3\times1}$, respectively. The sensing terminal implements L measurement channels, for all Tx-Rx antenna pairs (say, each single antenna is located in $\mathbf{x}_{\mathrm{T},\ell}$ and $\mathbf{x}_{\mathrm{R},\ell}$, respectively). At each Tx antenna, the sensing terminal emits the signal

$$s(t) = g(t)e^{j2\pi f_0 t} \tag{1}$$

where the base-band waveform $g(t)$ has bandwidth B and the carrier frequency is f_0. For simplicity, we assume $g(t)$ to be the same on each Tx antenna, as for a MIMO radar operating in time-division multiplexing. The RIS is in the generic position $\mathbf{x} \in \mathbb{R}^{3\times1}$ and is made by $N \times M$ elements, displaced along the x and y axes of the *local* reference system. The local axes are rotated w.r.t. the global ones by the Euler angles $\boldsymbol{\gamma} = [\psi_x, \psi_y, \psi_z]^T \in \mathbb{R}^{3\times1}$ (roll ψ_x, pitch ψ_y and yaw ψ_z). These latter represent the RIS orientation, which is the objective of the estimation together with position $\mathbf{x}$. The position of the (n,m)-th element of the RIS in global coordinates is

$$\mathbf{x}_{nm} = \mathbf{x} + \mathbf{Q}(\boldsymbol{\gamma})\mathbf{p}_{nm} \tag{2}$$

for $n = -N/2, ..., N/2 - 1$, $m = -M/2, ..., M/2 - 1$, where $\mathbf{p}_{nm} = [nd, md, 0]^\mathrm{T}$ is the local position of the (n,m)-th element in local coordinates (for inter-element spacing d), matrix $\mathbf{Q}(\boldsymbol{\gamma}) = \mathbf{Q}_z(\psi_z)\mathbf{Q}_y(\psi_y)\mathbf{Q}_x(\psi_x) \triangleq \{\mathbf{Q}|\det(\mathbf{Q}) = 1, \mathbf{Q}\mathbf{Q}^T = \mathbf{I}_3\}$ defines the relative counterclockwise rotation of the local reference system around z, y and x axis by angles ψ_z, ψ_y, ψ_x, respectively, where single cascaded rotation matrices are defined according to the convention indicated in Fig. 1.

The Rx signal for the ℓ-th measurement channel of the sensing terminal (after demodulation) is reported in (3) expressed in the frequency domain, where ρ denotes geometrical energy losses, $G(f)$ is the Fourier transform of $g(t)$, Φ_{nm} is the phase applied at the (n,m)-th element of the RIS,

$$\tau^i_{\ell,nm} = \frac{\|\mathbf{x}_{nm} - \mathbf{x}_{\mathrm{T},\ell}\|}{c}, \quad \tau^o_{\ell,nm} = \frac{\|\mathbf{x}_{\mathrm{R},\ell} - \mathbf{x}_{nm}\|}{c}, \tag{4}$$

are the absolute delays between the ℓ-th Tx and Rx antennas and the (n,m)-th element of the RIS, respectively. Term

$Z_\ell(f) \in \mathcal{CN}(0, N_0\delta_{\ell-k}\delta(f))$ is the additive noise with power spectral density N_0, while $H_\ell(f, \boldsymbol{\eta}|\boldsymbol{\Phi})$ is the deterministic component of the observation at the ℓ-th channel, function of the parameters to be estimated $\boldsymbol{\eta} = [\mathbf{x}, \boldsymbol{\gamma}]^T$ (RIs position and orientation) and of the RIS phases $\boldsymbol{\Phi} \in \mathbb{C}^{NM\times1}$. The expression of ρ follows from the radar equation [10]:

$$\rho = \sqrt{\frac{c^2}{(4\pi)^3 f_0^2 \|\mathbf{x} - \mathbf{x}_\mathrm{T}\|^2 \|\mathbf{x}_\mathrm{R} - \mathbf{x}\|^2} \Gamma_\mathrm{elem}} \; e^{j\delta} \tag{5}$$

where Γ_elem is the radar cross-section of the single RIS element of size d^2, and δ models residual phase uncertainties about the target (the RIS) arising, for instance, from Tx-Rx circuitry and Doppler effects from motion. We assume that Tx and Rx antennas, as well as RIS elements, are isotropic for simplicity.

Approximation (a) in (3) assumes FF at both RIS and sensing terminal, i.e., uniform planar wavefronts, thus the delays can be linearized as

$$\tau^i_{\ell,nm} \overset{(a)}{\simeq} \tau^i_0 + \Delta\tau^i_\ell(\boldsymbol{\zeta}_\mathrm{T})) + \Delta\tau^i_{nm}(\boldsymbol{\xi}_i) \tag{6}$$

$$\tau^o_{\ell,nm} \overset{(a)}{\simeq} \tau^o_0 + \Delta\tau^o_\ell(\boldsymbol{\zeta}_\mathrm{R}) + \Delta\tau^o_{nm}(\boldsymbol{\xi}_o) \tag{7}$$

where τ^i_0 and τ^o_0 are the macroscopic delays between the Tx and Rx phase centers and the RIS phase center, respectively, while $\Delta\tau^i_\ell$ and $\Delta\tau^o_\ell$ are the excess delays at the sensing terminal, function of angles of departure and arrivals $\boldsymbol{\zeta}_\mathrm{T}$ and $\boldsymbol{\zeta}_\mathrm{R}$ respectively, whereas $\Delta\tau^i_{nm}$ and $\Delta\tau^o_{nm}$ are the excess delays at the RIS, function of incidence and reflection angles $\boldsymbol{\xi}_i = [\phi_i, \theta_i]^T = J(\mathbf{Q}(\boldsymbol{\gamma})(\mathbf{x}_\mathrm{T} - \mathbf{x}))$ and $\boldsymbol{\xi}_o = [\phi_o, \theta_o]^T = J(\mathbf{Q}(\boldsymbol{\gamma})(\mathbf{x}_\mathrm{R} - \mathbf{x}))$ (elevation and azimuth), where $J : \mathbb{R}^{3\times1} \to \mathbb{R}^{2\times1}_{2\pi}$ is the transformation between global Cartesian coordinates to RIS-local spherical coordinates, according to the convention in Fig. 1. In FF, the overall RIS behavior is summarized by factor

$$\beta(f|\boldsymbol{\Phi}) = \rho \sum_{n,m} e^{j\Phi_{nm}} e^{-j2\pi(f_0+f)(\Delta\tau^i_{nm} + \Delta\tau^o_{nm})}, \tag{8}$$

that is the overall frequency-dependent RIS reflection coefficient (including path loss). The base-band frequency $f \in [-B/2, B/2]$ models the spatially wideband response of the RIS through $\beta(f|\boldsymbol{\Phi})$, that *filters* the impinging signal $G(f)$.

The further approximation (b) in (3) assumes narrowband operation, i.e., the duration $1/B$ of the base-band Tx waveform $g(t)$ is not affected by the residual (excess) delays at the RIS and at the sensing terminal. In other words, the narrowband approximation in the frequency domain implies that the RIS has the same reflection coefficient for all the frequencies f (corresponding to f_0). The narrowband operation is currently assumed in all the literature [7,8] but does not practically match the reality in most of sensing acquisitions. In the following, we derive and compare the CRB for the model (3), highlighting the spatially wideband effects.

8962

$$Y_\ell(f) = \rho\, G(f) \underbrace{\sum_{n,m} e^{j\Phi_{nm}} e^{-j2\pi(f_0+f)(\tau_{\ell,nm}^i + \tau_{\ell,nm}^o)}}_{H_\ell(f,\boldsymbol{\eta}|\boldsymbol{\Phi})} + Z_\ell(f)$$

$$\stackrel{(a)}{\approx} G(f) e^{-j2\pi(f_0+f)(\tau_0^i + \tau_0^o + \Delta\tau_\ell^i + \Delta\tau_\ell^o)} \beta(f|\boldsymbol{\Phi}) + Z_\ell(f) \stackrel{(b)}{\approx} G(f) e^{-j2\pi(f_0+f)(\tau_0^i + \tau_0^o)} e^{-j2\pi f_0(\Delta\tau_\ell^i + \Delta\tau_\ell^o)} \beta(0|\boldsymbol{\Phi}) + Z_\ell(f) \tag{3}$$

3. CRB ON POSITION AND ORIENTATION

The CRB is evaluated by assuming the knowledge of ρ (path-loss), that allows obtaining an optimistic lower bound on position and orientation estimation. If ρ is unknown, its real and imaginary parts can be included in the parameters to be estimated, increasing the CRB. The RIS can be configured according to [11]:

$$[\overline{\boldsymbol{\Phi}}]_{nm} = \begin{cases} 2\pi f_0 \left[\dfrac{\|\mathbf{x}_{nm} - \mathbf{x}_T\|}{c} + \dfrac{\|\mathbf{x}_R - \mathbf{x}_{nm}\|}{c} \right] & \text{NF} \\ 2\pi f_0 \left[\Delta\tau_{nm}^i + \Delta\tau_{nm}^o \right] & \text{FF} \end{cases} \tag{9}$$

where in the first case (NF) the RIS is able to perfectly focus the impinging radiation towards the phase center of the sensing terminal, while in the second case (FF) the RIS is configured to reflect the signal from $\boldsymbol{\xi}_i$ to $\boldsymbol{\xi}_o$. The perfect RIS configuration represents an upper performance bound modeling the situation in which the RIS follows some focusing alignment procedure such as the one in [12], not necessarily implying the perfect knowledge of $\mathbf{x}$ and $\boldsymbol{\gamma}$ (and thus of $\mathbf{x}_{nm}$), which is the objective of the estimation. A similar consideration can be made for FF configuration. In any case, the NF/FF phase configuration is optimal only at f_0. The Fisher information matrix (FIM) $\mathbf{F}$ is block-partitioned as follows:

$$\mathbf{F} = \begin{bmatrix} \mathbf{F_{xx}} & \mathbf{F_{x\gamma}} \\ \mathbf{F_{\gamma x}} & \mathbf{F_{\gamma\gamma}} \end{bmatrix} \tag{10}$$

with straightforward dimensions, whose entries are

$$[\mathbf{F}]_{ij} = \frac{2}{N_0} \Re \left\{ \sum_{\ell=1}^{L} \int_B \frac{\partial H_\ell^*(f,\boldsymbol{\eta}|\overline{\boldsymbol{\Phi}})}{\partial[\boldsymbol{\eta}]_i} \frac{\partial H_\ell(f,\boldsymbol{\eta}|\overline{\boldsymbol{\Phi}})}{\partial[\boldsymbol{\eta}]_j} df \right\} \tag{11}$$

where the integral is over the occupied bandwidth B and the summation of over the measurement channels L.

4. NUMERICAL RESULTS

We show numerical results quantifying the spatially wideband effects for the position and orientation estimation of a target-lodged RIS. We consider a monostatic sensing terminal operating at $f_0 = 78.5$ GHz, on a variable bandwidth $B \in [1, 10]$ GHz, equipped with 1 Tx antenna located in the origin of the global coordinate system and 20×20 Rx antennas along y

and z axes. The RIS size is variable, from $A_{\text{ris}} = 5 \times 5$ cm^2 to $A_{\text{ris}} = 35 \times 35$ cm^2. In all the evaluations, the RIS is in $\mathbf{x} = [5, 0, -5.5]^T$ m, located on the xy plane, for example, the RIS is mounted on a vehicle roof and illuminated by radar on a roadside unit. The Tx power is 23 dBm at the single Tx antenna, and the Rx signal is corrupted by thermal noise with $N_0 = -173$ dBm/Hz. Notice that, as the power is kept fixed, increasing the bandwidth B means decreasing the energy spectral density of the Tx signal $G(f)$.

The first result is summarized in Fig. 2. We show the position error bound (PEB), evaluated as

$$\text{PEB} = \sqrt{\frac{\text{trace}([\mathbf{F}^{-1}]_{1:3,1:3})}{3}} \tag{12}$$

(a)

(b)
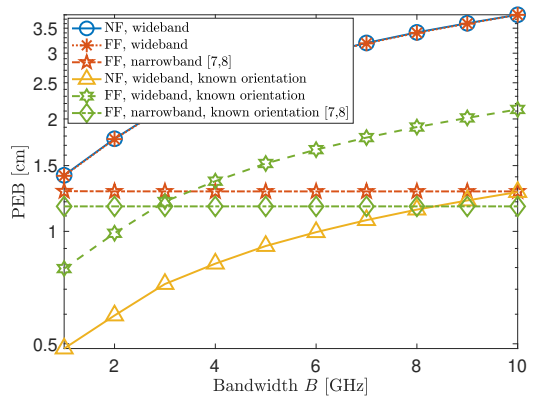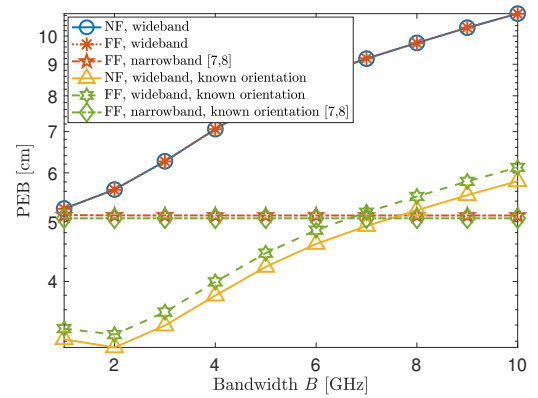
Fig. 2: PEB vs. B for (a) 10×10 cm^2 and (b) 20×20 cm^2 RIS. The narrowband model is commonly considered in literature [7,8].

8963

where the FIM can be either the NF or the FF one, under either spatially wideband or narrowband operation. The latter, being the current state of the art [7, 8], assumes that the RIS behavior is independent on the base-band frequency f, as for approximation (b) in (3). We also report as a benchmark the lower bound in which the orientation $\boldsymbol{\gamma}$ is known (or its estimation is assumed to be decoupled from position), thus $\mathbf{F} = \mathbf{F_{xx}}$. Let us first consider the case of a 10×10 cm^2 RIS (Fig. 2a). For increasing bandwidth B, the PEB increases as well, as long as the spatially wideband modeling (both NF and FF) is concerned. PEB for narrowband FF is invariant, and it lower bounds the spatially wideband one, underestimating the true PEB. The former effect is counter intuitive, as increasing B is expected to decrease the PEB thanks to an increase in the sensing resolution. This is not true, as the RIS in spatially wideband conditions operates as a *filter* on the Tx signal spectrum $G(f)$ that actually decreases the reflected energy w.r.t. the narrowband (frequency-flat) case. Notice that even when the RIS is assumed to be not frequency-selective (FF, narrowband curve), the PEB does not improve with B, as the effective bandwidth of $s(t)$ (1) is [13]:

$$B_{\text{eff}}^2 = f_0^2 + \frac{B^2}{12} \approx f_0^2, \qquad (13)$$

is largely dominated by the carrier component for the considered settings, and almost insensitive to B (for $B = 10$ GHz and $f_0 = 78.5$ GHz, the first term of (13) is 3 orders of magnitude higher than the second). This is common for carrier-phase positioning [14]. Fig. 2a also highlights the difference between the NF and FF modeling of the RIS behavior. When the orientation $\boldsymbol{\gamma}$ is known, e.g., an RIS is deployed on the rooftop of a vehicle, the FF shows higher PEB, as expected, as NF enables energy focusing at the Rx side.

Interestingly, for known $\boldsymbol{\gamma}$, the spatially wideband PEB can be lower than the narrowband one. Thus, the information brought in the FIM by the position-dependent filtering operated by the RIS overcomes the energy loss due to beam squinting and yields lower PEB. As B increases, the energy loss becomes dominant, and spatially wideband PEB starts to be larger than the narrowband one (i.e., the NF/FF spatially
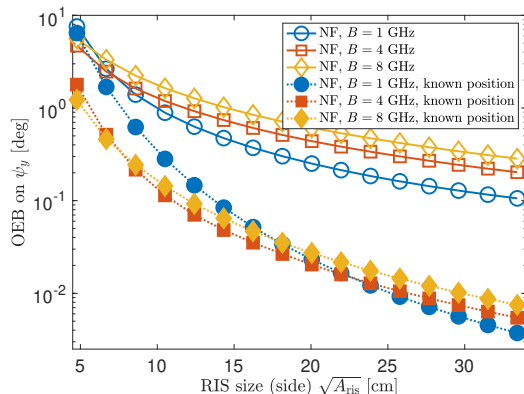
Fig. 3: OEB of ψ_y vs. RIS size (side size).

wideband PEB curves cross the FF narrowband one). This latter threshold effect depends on the size of the RIS and on its distance from the sensing terminal. Although not reported for brevity, it can be shown that as the latter increases, the information loss due to spatial energy spreading dominates over the pose-dependent filtering effect, shifting the threshold towards lower values of B. This phenomenon is also observed by increasing the size of the RIS (see Fig. 2b). In this latter case, the PEB gap between NF and FF—with $\boldsymbol{\gamma}$ known—is higher, whereas again no difference between NF and FF is observed for the position estimation problem.

The second result, in Fig. 3, reports the orientation error bound (OEB) on the pitch angle ψ_y for the NF spatially wideband model, versus the RIS size, varying the bandwidth $B = 1, 4, 8$ GHz. The OEB is defined as

$$\text{OEB}_y = \sqrt{[\mathbf{F}^{-1}]_{5,5}} \qquad (14)$$

where the lower bound corresponding to known position $\mathbf{x}$ is obtained by plugging $\mathbf{F} = \mathbf{F_{\gamma\gamma}}$ in (14). We select the pitch angle ψ_y to be analyzed as it is the one providing the lower OEB among ψ_x, ψ_y, ψ_z, thus the higher model sensitivity. We notice that increasing the size of the RIS means increasing its frequency-selectivity for a given bandwidth B (narrowing its reflection beamwidth and exacerbating the spatially wideband effect), thus penalizing the Rx signal energy. The result is an OEB that worsens with B except for a very small RIS. For known $\mathbf{x}$, instead, this latter effect is only observed above a given RIS size, approximately 20×20 cm^2 in the considered settings. Below, the lower OEB value is attained by $B = 4$ GHz, as a trade-off between frequency-selectivity (dominating for large B) and a beneficial *pose-dependent filtering* (dominating for small B). This is a further confirmation of what is observed on the PEB in Fig. 2, and underlines the importance of the spatially wideband modeling in the position and orientation estimation of a target-lodged RIS.

5. CONCLUSION

This paper analyzes the spatially wideband effects on the position plus orientation estimation of a RIS (that can be possibly placed on a desired target), namely the frequency-dependent (filter) RIS behavior when the employed sensing signal bandwidth is large. We derive the CRB in NF/FF and wideband/narrowband modeling assumptions, discussing the trend of PEB and OEB varying the employed bandwidth and RIS size, respectively. The results highlight the importance of spatially wideband modeling of the RIS for localization, and, under some circumstances and typical NF conditions, the spatially wideband PEB is tighter than the narrowband one, as the RIS behaves like a pose-dependent filter. Further, the spatially wideband RIS behavior opens for further research on the optimal spectral shaping of $G(f)$ to optimize (lower) the PEB/OEB.

6. REFERENCES

[1] Marco Di Renzo, Alessio Zappone, Merouane Debbah, Mohamed-Slim Alouini, Chau Yuen, Julien De Rosny, and Sergei Tretyakov, "Smart radio environments empowered by reconfigurable intelligent surfaces: How it works, state of research, and the road ahead," *IEEE Journal on Selected Areas in Communications*, vol. 38, no. 11, pp. 2450–2525, 2020.

[2] Hongliang Zhang, Boya Di, Kaigui Bian, Zhu Han, H. Vincent Poor, and Lingyang Song, "Toward ubiquitous sensing and localization with reconfigurable intelligent surfaces," *Proceedings of the IEEE*, vol. 110, no. 9, pp. 1401–1422, 2022.

[3] Stefano Buzzi, Emanuele Grossi, Marco Lops, and Luca Venturino, "Foundations of mimo radar detection aided by reconfigurable intelligent surfaces," *IEEE Transactions on Signal Processing*, vol. 70, pp. 1749–1763, 2022.

[4] Haobo Zhang, Hongliang Zhang, Boya Di, Kaigui Bian, Zhu Han, and Lingyang Song, "Metalocalization: Reconfigurable intelligent surface aided multi-user wireless indoor localization," *IEEE Transactions on Wireless Communications*, vol. 20, no. 12, pp. 7743–7757, 2021.

[5] Davide Dardari, Nicoló Decarli, Anna Guerra, and Francesco Guidi, "Los/nlos near-field localization with a large reconfigurable intelligent surface," *IEEE Transactions on Wireless Communications*, vol. 21, no. 6, pp. 4282–4294, 2022.

[6] Mingan Luan, Bo Wang, Yanping Zhao, Zhiyuan Feng, and Fengye Hu, "Phase design and near-field target localization for ris-assisted regional localization system," *IEEE Transactions on Vehicular Technology*, vol. 71, no. 2, pp. 1766–1777, 2022.

[7] Peilan Wang, Weidong Mei, Jun Fang, and Rui Zhang, "Target-mounted intelligent reflecting surface for joint location and orientation estimation," 2023.

[8] Reza Ghazalian, Kamran Keykhosravi, Hui Chen, Henk Wymeersch, and Riku Jäntti, "Bi-static sensing for near-field ris localization," in *GLOBECOM 2022 - 2022 IEEE Global Communications Conference*, 2022, pp. 6457–6462.

[9] Kamran Keykhosravi, Musa Furkan Keskin, Gonzalo Seco-Granados, Petar Popovski, and Henk Wymeersch, "Ris-enabled siso localization under user mobility and spatial-wideband effects," *IEEE Journal of Selected Topics in Signal Processing*, vol. 16, no. 5, pp. 1125–1140, 2022.

[10] Merrill Skolnik, *Introduction to Radar Systems*, McGraw-Hill Education, London, 2002.

[11] Dario Tagliaferri, Marouan Mizmizi, Giacomo Oliveri, Umberto Spagnolini, and Andrea Massa, "Reconfigurable and static em skins on vehicles for localization," 2023.

[12] Ahmed Elzanaty, Anna Guerra, Francesco Guidi, and Mohamed-Slim Alouini, "Reconfigurable intelligent surfaces for localization: Position and orientation error bounds," *IEEE Transactions on Signal Processing*, vol. 69, pp. 5386–5402, 2021.

[13] U. Spagnolini, *Statistical Signal Processing in Engineering*, John Wiley & Sons Ltd, 2018.

[14] Henk Wymeersch, Rouhollah Amiri, and Gonzalo Seco-Granados, "Fundamental performance bounds for carrier phase positioning in cellular networks," 2023.